Rapid Communications

$NaYbS_2$: A planar spin-$\frac{1}{2}$ triangular-lattice magnet and putative spin liquid

M. Baenitz,[1,*] Ph. Schlender,[2] J. Sichelschmidt,[1] Y. A. Onykiienko,[3] Z. Zangeneh,[4] K. M. Ranjith,[1] R. Sarkar,[3] L. Hozoi,[4] H. C. Walker,[5] J.-C. Orain,[6] H. Yasuoka,[1] J. van den Brink,[4] H. H. Klauss,[3] D. S. Inosov,[3] and Th. Doert[2]

[1]*Max Planck Institute for Chemical Physics of Solids, D-01187 Dresden, Germany*
[2]*Faculty of Chemistry and Food Chemistry, TU Dresden, D-01062 Dresden, Germany*
[3]*Institute for Solid State and Materials Physics, TU Dresden, D-01062 Dresden, Germany*
[4]*Leibniz Institute for Solid State and Materials Research, IFW Dresden, D-01069 Dresden, Germany*
[5]*ISIS Neutron and Muon Source, Rutherford Appelton Laboratory, Chilton, Didcot OX11 OQX, United Kingdom*
[6]*Laboratory for Muon Spin Spectroscopy, Paul Scherrer Institute, CH-5232 Villingen PSI, Switzerland*

(Received 6 September 2018; revised manuscript received 13 November 2018; published 26 December 2018)

Platelike high-quality $NaYbS_2$ rhombohedral single crystals with lateral dimensions of a few mm have been grown and investigated in great detail by bulk methods such as magnetization and specific heat, but also by local probes such as nuclear magnetic resonance (NMR), electron-spin resonance (ESR), muon-spin relaxation (μSR), and inelastic neutron scattering over a wide field and temperature range. Our single-crystal studies clearly evidence a strongly anisotropic quasi-two-dimensional magnetism and an emerging spin-orbit entangled $J_{\rm eff} = \frac{1}{2}$ state of Yb towards low temperatures together with an absence of long-range magnetic order down to 260 mK. In particular, the clear and narrow Yb ESR lines together with narrow ^{23}Na NMR lines evidence an absence of inherent structural distortions in the system, which is in strong contrast to the related spin-liquid candidate $YbMgGaO_4$ falling within the same space group $R\bar{3}m$. This identifies $NaYbS_2$ as a rather pure spin-$\frac{1}{2}$ triangular-lattice magnet and a putative quantum spin liquid.

DOI: 10.1103/PhysRevB.98.220409

Introduction. In low-dimensional quantum magnets, competing confined magnetic exchange interactions restrict the magnetic degrees of freedom, which leads to a strong frustration accompanied by enhanced quantum fluctuations. Ultimately this prevents the systems from long-range order, and the ground state is supposed to be a magnetic liquid. There are various types of such quantum spin liquids (QSLs) depending on the lattice geometry [in two dimensions (2D): square, triangular, kagome, or honeycomb type; in three dimensions (3D): hyperkagome, hyperhoneycomb, or pyrochlore], the magnetic exchange (e.g., Heisenberg, Kitaev, or Dzyaloshinskii-Moriya type), and the magnetic ion itself [1–4]. Planar spin-$\frac{1}{2}$ triangular-lattice magnets (TLMs) with antiferromagnetic exchange interactions are ideal QSL candidates as proposed by Anderson [5]. A few examples are found among the organic materials, such as κ-$(BEDT\text{-}TTF)_2Cu_2(CN)_3$ [6] and $Et_nMe_{4-n}Sb[Pd(DMIT)_2]_2$ [7], whereas among inorganic compounds such QSL model systems are very rare, e.g., $Ba_3CuSb_2O_9$ [8].

For TLMs the fingerprint of the emerging $U(1)$-QSL state is the formation of the gapless spinon Fermi surface evidenced by a finite and constant magnetic specific-heat coefficient $C_{\rm m}/T$ and a finite residual magnetic susceptibility [2–4,9]. Persisting low-energy magnetic excitations with characteristic dispersion relations could be evidenced by inelastic neutron scattering (INS), nuclear magnetic resonance (NMR), and muon spin relaxation (μSR) [2–4,6,10,11]. Recently, the field of $S = \frac{1}{2}$ quantum magnetism was extended away from $3d$ ions (such as Cu^{2+} and V^{4+}) towards $4d$, $5d$, and even $4f$ systems [2]. In these materials, an effective $J_{\rm eff} = \frac{1}{2}$ moment can be realized due to strong spin-orbit coupling (SOC). The honeycomb $4d$ and $5d$ QSL candidates α-$RuCl_3$ and Na_2IrO_3 are *proximate QSLs* [12] and exhibit long-range order, whereas the $4f$-TLM $YbMgGaO_4$ is claimed to be a gapless QSL with an absence of order and persistent magnetic excitations down to the lowest temperatures [11,13–17]. The strong spin-orbit interaction could be at the same energy scale as the Coulomb interaction U and the crystal electric field (CEF) splitting, which finally leads to highly degenerate bandlike magnetic states with complex excitations [18]. Especially for the $4f$-TLMs (based on Ce or Yb), the spin-orbit entanglement leads to highly anisotropic bond-dependent interactions among the moments, which should strongly enhance quantum fluctuations and promote a QSL ground state [15,19–24]. In the absence of SOC, the classical $S = \frac{1}{2}$ isotropic Heisenberg model predicts the energy-minimum solution to be the planar 120° Néel-ordered state with a strong magnetic anisotropy [25–28]. An additional next-nearest-neighbor interaction could quench the 120° order and drive the system towards a QSL or an antiferromagnetic stripe phase [29]. As the first QSL-TLM with a strong $4f$-driven SOC, $YbMgGaO_4$ gained a lot of attention, but it turned out that there is a considerable site mixing between Ga and Mg ions, which affects the magnetic properties in general and the predicted QSL ground state in particular [30,31]. As for Yb-TLMs, the SOC of the Yb ion and the CEF create a ground-state doublet which at low temperatures could be described with an effective spin of

*Corresponding author: michael.baenitz@cpfs.mpg.de

$\frac{1}{2}$, and any structural distortion consequently alters the CEF splitting and may strongly affect the magnetic ground state [17,31].

In the search for the ideal spin-$\frac{1}{2}$ TLM with a spin-orbit interaction, we focused on the $A^{1+}R^{3+}X_2$ delafossites, where A is a nonmagnetic monovalent metal ion, R is a rare-earth ion (Ce or Yb), and X stands for either oxygen or sulfur. Most of them form in the same $R\bar{3}m$ space group as $YbMgGaO_4$, and most importantly they exhibit perfect triangular layers of R^{3+} ions, composed of edge-sharing RO_6 octahedra. In contrast to $YbMgGaO_4$, all R^{3+} ions in the delafossite structure reside at one single site which is an inversion center of the structure and the center of the RO_6 octahedra. Furthermore, delafossites have an ABAB stacking of the triangular layers along the c axis, in contrast to the ABCABC stacking in $YbMgGaO_4$. Among the delafossites, there are some early reports on $AYbO_2$ (A = Ag, Na) polycrystals that suggest a pseudospin $J_{\text{eff}} = \frac{1}{2}$ ground state [32–34]. So far no single crystals were accessible for these systems, whereas there is a report about the single-crystal growth of the sulfur homolog $NaYbS_2$ [35]. We succeeded in the synthesis of sizable platelike high-quality single crystals and our comprehensive study combines bulk methods, local probes, and quantum chemistry calculations. $NaYbS_2$ is a spin-orbit entangled $J_{\text{eff}} = \frac{1}{2}$ TLM and putative QSL hosted on a perfect triangular lattice.

Experimental techniques. We have grown $NaYbS_2$ single crystals by a modified method following Lissner and Schleid [35], starting from rare-earth metal grains, sulfur, and sodium chloride as the flux. After the reactions the water-insoluble product was washed with water and ethanol and dried at 60 °C. The single crystals form as transparent yellowish thin (∼100-μm) platelets with lateral dimensions up to 10 mm. For polycrystalline samples of $NaYbS_2$ and $NaLuS_2$, a salt metathesis was used, starting from rare-earth trichloride and sodium sulfide ground together with excess of sodium chloride as the flux, as detailed in the Supplemental Material (SM) [36]. $NaYbS_2$ forms in the rhombohedral α-$NaFeO_2$ delafossite structure ($R\bar{3}m$) with $a = 3.895(1)$ Å and $c = 19.831(6)$ Å [35,53,54]. Magnetization measurements were performed with superconducting quantum interference device (SQUID) magnetometers [magnetic property measurement system (MPMS), vibrating sample magnetometer (VSM)] and an ac/dc susceptometer [physical property measurement system (PPMS)] from Quantum Design. The MPMS was equipped with a ^{3}He cooling stage (down to 500 mK) and the VSM was equipped with a goniometer to probe the angular dependence of the magnetization [36]. Specific-heat measurements were conducted with a commercial PPMS from Quantum Design down to 350 mK. NMR measurements were carried out by applying conventional pulsed NMR in the field-sweep mode on both powder and single crystals [36]. μSR experiments down to 260 mK were performed at the Paul Scherrer Institute (DOLLY instrument) on sandwiched $NaYbS_2$ single crystals (48 mg). INS measurements were performed on the polycrystalline $NaYbS_2$ material (6 g) at the thermal-neutron time-of-flight (TOF) spectrometer MERLIN at ISIS Neutron and Muon Source [55,56]. Electron-spin resonance (ESR) experiments were performed at X- and Q-band frequencies (9.4 and 34 GHz) on single crystals and powders down to liquid-helium temperatures [57].

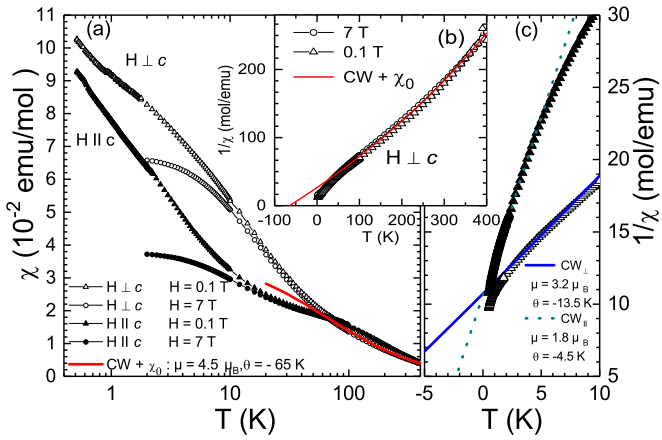

FIG. 1. (a) Temperature dependence of the magnetic susceptibility ($\chi_\parallel$ and $\chi_\perp$) of $NaYbS_2$ measured in $H = 7$ and 0.1 T. The solid line corresponds to an extended Curie-Weiss fit which includes an additional small diamagnetic offset contribution ($\chi_0 = -0.0015$ emu/mol). (b) Inverse susceptibility $1/\chi_\perp$ and extended CW fit to the data between 80 and 400 K (solid line). (c) Inverse susceptibilities below 10 K and CW fits to the data (solid and dotted lines).

Results. Figure 1(a) shows the susceptibility of $NaYbS_2$ as a function of temperature in 0.1 and 7 T for the fields H applied in the (a, b) plane, $\chi_\perp(T, H)$, and along the c direction, $\chi_\parallel(T, H)$. Above 80 K the magnetic anisotropy disappears, and the field dependence becomes negligible. Here, the susceptibility $\chi(T)$ could be fitted well (after the subtraction of a small T-independent diamagnetic contribution χ_0) with a Curie-Weiss (CW) law, which yields a Weiss temperature of $\theta = -65$ K and an effective moment of $\mu_{\text{eff}} = 4.5\mu_B$ [Fig. 1(b)]. The CW fit parameters are similar to those obtained from polycrystalline powder [36], and the μ_{eff} value agrees with the theoretical prediction for trivalent Yb with $J = \frac{7}{2}$ ($4.54\mu_B$). Furthermore, these values are rather similar to findings on $AgYbO_2$ powder samples [34]. Below 80 K a sizable magnetic anisotropy develops, and there is a strong field effect on the susceptibility which indicates an emerging effective low-spin state with a small exchange coupling. Plotting the inverse susceptibility $1/\chi_\perp(T)$ (measured down to 0.5 K) at 0.1 T below 10 K clearly shows a CW behavior with $\mu_{\text{eff}\perp} = 3.2\mu_B$ and $\theta_\perp = -13.5$ K [Fig. 1(c)] down to about 1 K. Below 1 K, $1/\chi_\perp(T)$ bends over into a behavior with an even smaller moment. For the field in the c direction, below 10 K, $1/\chi_\parallel(T)$ is still curved, but fitting a CW law below approximately 5 K provides a moment of $\mu_{\text{eff}\parallel} = 1.8\mu_B$, and a Weiss temperature of $\theta_\parallel = -4.5$ K. The low-T susceptibility clearly evidences a SOC entangled enhancement of the magnetic moment in plane ($3.2\mu_B$), whereas out of plane the CW moment is strongly reduced. Below 1 K it seems that both $1/\chi(T)$ curves tend to merge. The fact that there is no magnetic order above 0.26 K allows an estimate of a lower limit for the frustration parameter which is $f = \theta_\perp/(0.26\text{ K}) = 52$ in the (a, b) plane and $f = \theta_\parallel/(0.26\text{ K}) = 17$ in the c direction.

The magnetization $M(H)$ was measured for $\mathbf{H} \parallel \mathbf{c}$ and $\mathbf{H} \perp \mathbf{c}$ in fields up to 14 T at $T = 2$ K (for powder data at 0.5 K, see SM [36]). Both magnetizations show no sign of saturation in that field range [Fig. 2(a)]. From the difference in the Weiss temperature and the anisotropy of μ_{eff}, the strongest

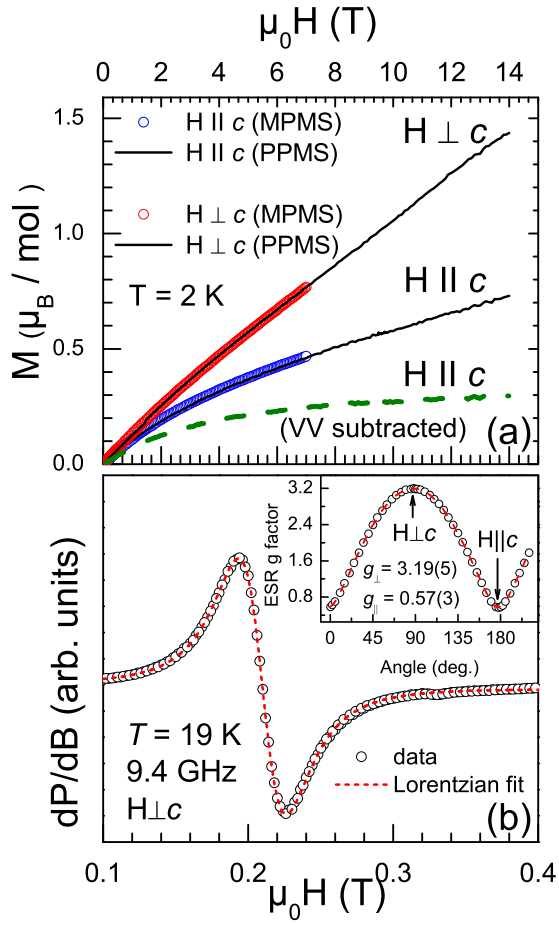

FIG. 2. (a) Magnetization vs field for $\mathbf{H} \parallel \mathbf{c}$ and $\mathbf{H} \perp \mathbf{c}$ at $T = 2$ K [open symbols and solid lines represent data from SQUID measurements (Quantum Design MPMS) and from dc-susceptometer measurements (Quantum Design PPMS), respectively]. The dashed line corresponds to $M_{\parallel}$-$H\chi_{\mathrm{VV}\parallel}$ (see text). (b) ESR line at 19 K (the dashed line corresponds to a Lorentzian fit). The inset shows the angular dependence of the ESR g-factor at 19 K (dashed line represents a uniaxial fit).

field effect on $M(H)$ is expected for $\mathbf{H} \parallel \mathbf{c}$. As a further probe for the anisotropy we applied ESR on the $NaYbS_2$ single crystal. A well-resolved and narrow Yb ESR line could be found for both orientations [Fig. 2(b)]. This is in strong contrast to $YbMgGaO_4$, where structural distortions (Mg-Ga site mixing, Yb sits on off-center positions in the YbO_6 octahedra [17,31]) lead to a CEF randomness resulting in a rather broad and much less resolved ESR line (with $g_{\perp} = 3.06$ and $g_{\parallel} = 3.72$) and a strong broadening of inelastic neutron CEF peaks [30]. The ESR g-factor in $NaYbS_2$ is strongly anisotropic (with $g_{\perp} = 3.19$ and $g_{\parallel} = 0.57$) and nearly T independent below approximately 50 K [57], which signals a large CEF anisotropy at the Yb ion [Fig. 2(b), inset]. In general, the g factors describe the Zeeman splitting of the lowest Kramers doublet of the Yb ion and depend on the local site symmetry and the character of the ground-state wave function [58]. Using the ESR g-factors we calculated the anisotropic moments of the ground-state doublet: $\mu_{\mathrm{ESR}} = \mathrm{g}\sqrt{J_{\mathrm{eff}}(J_{\mathrm{eff}}+1)}\mu_{\mathrm{B}} = 2.77\mu_{\mathrm{B}}$ for $\mathbf{H} \perp \mathbf{c}$ ($= 0.50\mu_{\mathrm{B}}$ for $\mathbf{H} \parallel \mathbf{c}$). These values deviate from the low-temperature CW

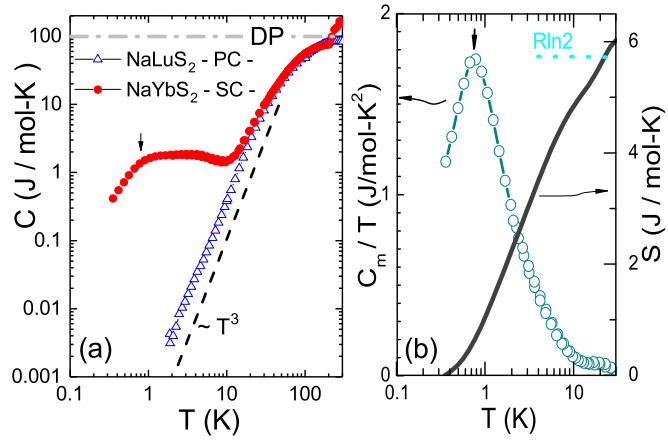

FIG. 3. (a) Temperature dependence of the specific heat of $NaYbS_2$ measured on stacked single crystals (SC) together with the nonmagnetic structural homologue $NaLuS_2$ [polycrystalline material (PC) as a pressed pellet]. The horizontal dashed line indicates the Dulong-Petit value (DP). (b) Magnetic heat capacity of $NaYbS_2$ divided by T as a function of temperature (left axis) and calculated entropy (right axis).

moments which could originate from an additional paramagnetic Van Vleck (VV) contribution in the susceptibility. In general, the VV contribution of a Yb^{3+} ion is associated with a second-order Zeemann effect due to the virtual excitations of higher CEF levels. As this contribution is hard to calculate it is rather difficult to account for this. From the ESR g values, saturation magnetizations of about $M_{\mathrm{sat}\perp} = \mathrm{g}_{\perp} J_{\mathrm{eff}} \mu_{\mathrm{B}} = 1.6\mu_{\mathrm{B}}$ and $M_{\mathrm{sat}\parallel} = \mathrm{g}_{\parallel} J_{\mathrm{eff}} \mu_{\mathrm{B}} = 0.285\mu_{\mathrm{B}}$ are expected. As seen in Fig. 2(a), $M_{\mathrm{sat}\parallel}(H)$ exceeds this estimate by more than a factor of 2, whereas in the (a, b) plane $1.6\mu_{\mathrm{B}}$ is not reached up to 14 T. Towards higher magnetic fields $M_{\parallel}$ might be dominated by the VV contribution which is linear in field ($M_{\parallel} = M_{\mathrm{sat}\parallel} + H\chi_{\mathrm{VV}\parallel}$) and reminiscent of other Yb systems (e.g., $YbRh_2Si_2$ [59]). Assuming a nearly complete saturation above 10 T yields a Van Vleck susceptibility of $\chi_{\mathrm{VV}\parallel} = 0.017$ emu/mol at 2 K and therefore allows for a first correction of $M(H)$ for $\mathbf{H} \parallel \mathbf{c}$ [Fig. 2(a)] [36]. The presence of a sizable VV contribution for $\mathbf{H} \parallel \mathbf{c}$ could also explain the curved behavior of $1/\chi_{\parallel}(T)$ [Fig. 1(c)]. An analysis of the susceptibility data assuming a constant VV contribution below 20 K recovers a linear $1/\chi_{\parallel}(T)$ behavior and yields a smaller moment of $\mu_{\mathrm{eff}\parallel,0} = 1.2\mu_{\mathrm{B}}$ ($\theta_{\parallel,0} = -1.8$ K) which is more consistent with the ESR moment determined above [36].

Specific-heat measurements have been performed on two single-crystalline $NaYbS_2$ samples [stacked single crystals of 15 mg total mass (Fig. 3) and a single crystal with a mass of 0.2 mg [36]] and polycrystalline $NaLuS_2$ as a nonmagnetic phonon reference between 350 mK and 300 K [Fig. 3(a)]. The magnetic contribution to the specific heat C_{m} is obtained by the subtraction of the phonon reference from the data. Figure 3(b) shows C_{m}/T together with the magnetic entropy. Although C_{m}/T vs T exhibits a peak at about $T^* = 0.8$ K, the entropy shows no anomaly at T^* and increases smoothly towards higher T, merging with the spin-$\frac{1}{2}$ value of $S \approx R \ln 2$ at about 20 K. The T^* peak is rather narrow in comparison to the hump found in $YbMgGaO_4$ at 2 K that originates from a (disorder-induced) Schottky effect [13]. As there are

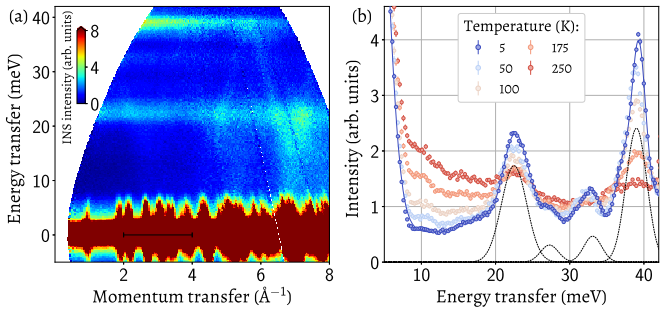

FIG. 4. (a) Powder TOF spectrum measured at 5 K with $E_i = 50$ meV. (b) The spectrum integrated over a momentum range of 2–4 Å^{-1} for various temperatures. The integration range is shown in (a) by the black interval. The black dashed line in (b) shows the individual peaks obtained from the fit of the 5-K data.

no signs of order in susceptibility (see Fig. 1) and μSR (where the relaxation rate stays constant below 1 K—see SM [36]), we speculate that the T^* peak signals the emerging QSL state probably with a partial gapping out of magnetic excitations [see, e.g., results on κ-(BEDT-TTF)$_2$Cu$_2$(CN)$_3$ [60]]. Another scenario is that persistent spin fluctuations do not completely suppress magnetic order, and the observed peak corresponds to a partial (probably short-range) magnetic order of a minor fraction of spins, whereas the majority part remains fluctuating. Nonetheless, in view of the susceptibility and preliminary μSR results, this appears unlikely. From the theory point of view the interaction between spin-orbit entangled Kramers-doublet local moments on planar triangles could be rather complex. Beside the classical 120° Néel phase and the QSL phase, complex magnetic textures such as stripes are predicted in the global phase diagram [15,21,22].

Further, we probed the CEF excitations of the Yb^{3+} ions by neutron spectroscopy. Figure 4(a) shows the TOF spectrum of the polycrystalline $NaYbS_2$ sample (6 g) at 5 K, measured with an incident neutron energy of $E_i = 50$ meV. Dispersing features that increase in intensity with increasing $|\mathbf{Q}|$ are associated with phonons, whereas horizontal lines with intensities decaying towards higher $|\mathbf{Q}|$ originate from CEF excitations. Figure 4(b) shows the integrated intensity between 2 and 4 Å^{-1} as a function of energy at several temperatures. The two most intense peaks at 23 and 39 meV share the same T dependence, which suggests that they are related to the CEF excitations of the $NaYbS_2$ material. Additional less intense peaks at 27 and 32 meV might originate from a minority phase in the sample (see discussion in the SM [36]). Nonetheless, in comparison with $YbMgGaO_4$, the INS peaks are rather narrow, which evidences the absence of inherent crystal-field randomness, in agreement with the narrow ESR lines. Furthermore, the CEF levels are found at lower energies compared to $YbMgGaO_4$ [17]. Making use of the $E_i = 131$ meV channel, we observed the spectra up to 100 meV, but we did not find any additional peaks. From the T-dependent ESR linewidth, the first excited CEF level is expected to be around 17 meV [57]. To cross check the values extracted from the ESR and INS measurements for the splittings among the low-lying Yb^{3+} f^{13} levels, we further performed *ab initio* quantum chemistry calculations using experimentally determined atomic positions (see details in SM [36]). We found low-lying excited states at 14, 20, and 47 meV with respect to the ground-state doublet, as well as computed ground-state g-factors of $g_\perp = 3.66$ and $g_\parallel = 0.60$. All these computational results are in reasonable agreement with the experimental INS and ESR data and provide a solid starting point for a more detailed analysis of the electronic structure of $NaYbS_2$.

Discussion. For spin-orbit coupled quasi-2D TLMs the extended XXZ model is established to capture the impact of the SOC [15,61]. Here, the interaction between the Kramers-doublet $J_{\text{eff}} = \frac{1}{2}$ moments is anisotropic in spin space and in real space. Therefore the interaction depends on the bond direction, which is a common feature among spin-orbit entangled QSLs (e.g., α-$RuCl_3$ and Na_2IrO_3). A complete estimate of the exchange constants is not possible with the data set presented. Nonetheless, from the Weiss constants $\theta_\perp = 3J^{+-} = -13.5$ K and $\theta_{\parallel,0} = (3/2)J^{zz} = -1.8$ K one could roughly estimate the standard XXZ model out-of-plane exchange $J^{zz} = -1.2$ K and the in-plane exchange $J^{+-} = -4.5$ K. These values evidence a rather two-dimensional magnetism which is in strong contrast to $YbMgGaO_4$(with $J^{zz} = -1.7$ K and $J^{+-} = -1$ K) [62]. The comparison of both systems is rather complex for the following reasons. First, the YbS_6 octahedron is larger than the corresponding YbO_6 octahedron in $YbMgGaO_4$ due to the difference in the ionic radii of S^{2-} and O^{2-} and the absence of (Mg/Ga)O_5 bipyramids [36]. Second, the Yb layer distance along the c axis is reduced for $NaYbS_2$ (6.57 Å vs 8.38 Å for $YbMgGaO_4$), and the a axis of $NaYbS_2$ is slightly larger, which finally leads to a 3.5% increase of the cell volume for $NaYbS_2$. Finally, in $NaYbS_2$, the Yb ion resides on a single site in the center of the YbS_6 octahedron which has an impact on the magnetic exchange. From that we conclude that the rhombohedral tilt of the $YbS(O)_6$ octahedron in the trigonal system is much more prominent in $NaYbS_2$ than in $YbMgGaO_4$ and causes both the g-factor anisotropy and the exchange anisotropy in the susceptibility. Furthermore, the c/a ratio of 5.1 for $NaYbS_2$ is smaller than that of 7.4 in $YbMgGaO_4$, which at first glance explains the relative shift of the CEF levels towards lower energies. In conclusion, our studies on $NaYbS_2$ clearly evidence a spin-orbit entangled anisotropic magnetism associated with the Kramers-doublet $J_{\text{eff}} = \frac{1}{2}$ local moment and the absence of inherent structural distortions. The combination of single-crystal magnetization and ESR evidences an exchange anisotropy and a strong g-factor anisotropy. Furthermore, single-crystal susceptibility, specific-heat, and μSR measurements evidence the absence of long-range magnetic order down to 260 mK. The planar TLM $NaYbS_2$ therefore could be regarded as a putative QSL candidate, and the data presented here will certainly stimulate more detailed future investigations in the mK regime on the complex ground state and its excitations.

Note added. Recently, we became aware of Ref. [63], where rare-earth chalcogenides in general are introduced as triangular-lattice QSL candidates.

We thank P. Gegenwart, A. Tsirlin, H. Rosner, B. Schmidt, and C. Geibel for fruitful discussions. Experiments at the ISIS Neutron and Muon Source were supported by a beamtime

allocation from the Science and Technology Facilities Council. We thank C. Klausnitzer and H. Rave for technical support during the magnetization and specific-heat measurements at the MPI. Z.Z. and L.H. acknowledge the DFG for financial support (Grant No. HO 4427/3). This work has been partially funded by the German Research Foundation (DFG) within the Collaborative Research Center SFB 1143 (Projects B03, C02, C03, and A05).

[1] P. A. Lee, Science **321**, 1306 (2008).
[2] L. Balents, Nature (London) **464**, 199 (2010).
[3] L. Savary and L. Balents, Rep. Prog. Phys. **80**, 016502 (2017).
[4] Y. Zhou, K. Kanoda, and T.-K. Ng, Rev. Mod. Phys. **89**, 025003 (2017).
[5] P. W. Anderson, Mater. Res. Bull. **8**, 153 (1973).
[6] Y. Shimizu, K. Miyagawa, K. Kanoda, M. Maesato, and G. Saito, Phys. Rev. Lett. **91**, 107001 (2003).
[7] M. Yamashita, N. Nakata, Y. Senshu, M. Nagata, H. M. Yamamoto, R. Kato, T. Shibauchi, and Y. Matsuda, Science **328**, 1246 (2010).
[8] H. D. Zhou, E. S. Choi, G. Li, L. Balicas, C. R. Wiebe, Y. Qiu, J. R. D. Copley, and J. S. Gardner, Phys. Rev. Lett. **106**, 147204 (2011).
[9] S.-S. Lee, P. A. Lee, and T. Senthil, Phys. Rev. Lett. **98**, 067006 (2007).
[10] T. Itou, A. Oyamada, S. Maegawa, and R. Kato, Nat. Phys. **6**, 673 (2010).
[11] Y. Shen, Y.-D. Li, H. Wo, Y. Li, S. Shen, B. Pan, Q. Wang, H. C. Walker, P. Steffens, M. Boehm, Y. Hao, D. L. Quintero-Castro, L. W. Harriger, M. D. Frontzek, L. Hao, S. Meng, Q. Zhang, G. Chen, and J. Zhao, Nature (London) **540**, 559 (2016).
[12] S. Trebst, Kitaev materials, in *Topological Matter–Topological Insulators, Skyrmions and Majoranas*, edited by S. Blügel, Z. Mokrousov, and T. Schäpers, Lecture Notes of the 48th IFF Spring School Vol. 139 (Schriften des Forschungszentrums Jülich, 2017).
[13] Y. Li, H. Liao, Z. Zhang, S. Li, F. Jin, L. Ling, L. Zhang, Y. Zou, L. Pi, Z. Yang, J. Wang, Z. Wu, and Q. Zhang, Sci. Rep. **5**, 16419 (2015).
[14] Y. Li, G. Chen, W. Tong, L. Pi, J. Liu, Z. Yang, X. Wang, and Q. Zhang, Phys. Rev. Lett. **115**, 167203 (2015).
[15] Y.-D. Li, X. Wang, and G. Chen, Phys. Rev. B **94**, 035107 (2016).
[16] J. A. M. Paddison, M. Daum, Z. Dun, G. Ehlers, Y. Liu, M. B. Stone, H. Zhou, and M. Mourigal, Nat. Phys. **13**, 117 (2017).
[17] Y. Li, D. Adroja, P. K. Biswas, P. J. Baker, Q. Zhang, J. Liu, A. A. Tsirlin, P. Gegenwart, and Q. Zhang, Phys. Rev. Lett. **117**, 097201 (2016).
[18] J. Knolle, *Dynamics of a Quantum Spin Liquid*, Springer Theses (Springer, New York, 2016).
[19] W.-J. Hu, S.-S. Gong, W. Zhu, and D. N. Sheng, Phys. Rev. B **92**, 140403 (2015).
[20] Y. Iqbal, W.-J. Hu, R. Thomale, D. Poilblanc, and F. Becca, Phys. Rev. B **93**, 144411 (2016).
[21] S.-S. Gong, W. Zhu, J.-X. Zhu, D. N. Sheng, and K. Yang, Phys. Rev. B **96**, 075116 (2017).
[22] Z.-Zhu, P. A. Maksimov, S.-R. White, and A. L. Chernyshev, Phys. Rev. Lett. **120**, 207203 (2018).
[23] J. Iaconis, C. Liu, G. B. Halasz, and L. Balents, SciPost Phys. **4**, 003 (2018).
[24] J. G. Rau and M. J. P. Gingras, Phys. Rev. B **98**, 054408 (2018).
[25] H. Kawamura and S. Miyashita, J. Phys. Soc. Jpn. **54**, 4530 (1985).
[26] A. V. Chubukov and D. I. Golosov, J. Phys.: Condens. Matter **3**, 69 (1991).
[27] D. Yamamoto, G. Marmorini, and I. Danshita, Phys. Rev. Lett. **112**, 127203 (2014).
[28] B. Schmidt and P. Thalmeier, Phys. Rep. **703**, 1 (2017).
[29] R. Kaneko, S. Morita, and M. Imada, J. Phys. Soc. Jpn. **83**, 093707 (2014).
[30] Y. Li, D. Adroja, R. I. Bewley, D. Voneshen, A. A. Tsirlin, P. Gegenwart, and Q. Zhang, Phys. Rev. Lett. **118**, 107202 (2017).
[31] I. Kimchi, A. Nahum, and T. Senthil, Phys. Rev. X **8**, 031028 (2018).
[32] Y. Hashimoto, M. Wakeshima, and Y. Hinatsu, J. Solid State Chem. **176**, 266 (2003).
[33] A. Saito, N. Sawaguchi, and M. Sasaki, J. Ceram. Soc. Jpn. **116**, 118 (2008).
[34] N. Miyasaka, Y. Doi, and Y. Hinatsu, J. Solid State Chem. **182**, 2104 (2009).
[35] T. Schleid and F. Lissner, Eur. J. Solid State Inorg. Chem. **30**, 829 (1993).
[36] See Supplemental Material at http://link.aps.org/supplemental/10.1103/PhysRevB.98.220409 for the details of sample preparation and results of additional measurements, which includes Refs. [37–52].
[37] H. J. Werner, P. J. Knowles, G. Knizia, F. R. Manby, and M. Schuetz, WIREs Comput. Mol. Sci. **2**, 242 (2012).
[38] T. Helgaker, P. Jorgensen, and J. Olsen, *Molecular Electronic-Structure Theory* (Wiley, Chichester, 2000).
[39] A. Berning, M. Schweizer, H. J. Werner, P. J. Knowles, and P. Palmieri, Mol. Phys. **98**, 1823 (2000).
[40] M. Dolg, H. Stoll, and H. Preuss, J. Chem. Phys. **90**, 1730 (1989).
[41] X. Cao and M. Dolg, J. Chem. Phys. **115**, 7348 (2001).
[42] X. Cao and M. Dolg, J. Mol. Struct. (Theochem) **581**, 139 (2002).
[43] D. E. Woon and T. H. Dunning, J. Chem. Phys. **98**, 1358 (1993).
[44] K. Pierloot, B. Dumez, P.-O. Widmark, and B. O. Roos, Theor. Chim. Acta **90**, 87 (1995).
[45] P. Fuentealba, H. Preuss, H. Stoll, and L. v. Szentpaly, Chem. Phys. Lett. **89**, 418 (1982).
[46] M. Dolg, H. Stoll, and H. Preuss, Theor. Chim. Acta **85**, 441 (1993).
[47] J. M. Baker and E. R. Davies, J. Phys. C: Solid State Phys. **8**, 1869 (1975).
[48] P. W. Atkins, M. S. Child, and C. S. G. Phillips, *Tables for Group Theory* (Oxford University Press, Oxford, UK, 1970).
[49] W. Li, G. Zhou, and T. Mak, *Advanced Structural Inorganic Chemistry* (Oxford University Press, Oxford, UK, 2008).

[50] M. Kresch, M. Lucas, O. Delaire, J. Y. Y. Lin, and B. Fultz, Phys. Rev. B **77**, 024301 (2008).
[51] A. Suter and B. Wojek, Phys. Proc. **30**, 69 (2012).
[52] R. Sarkar, J. Spehling, P. Materne, H. Luetkens, C. Baines, M. Brando, C. Krellner, and H.-H. Klauss, Phys. Rev. B **95**, 121111 (2017).
[53] K.-J. Range, W. Meister, and U. Klement, Z. Kristallogr. **207**, 145 (1993).
[54] J. P. Cotter, J. C. Fritzmaurice, and I. P. Parkin, J. Mater. Chem. **4**, 1603 (1999).
[55] R. I. Bewley, T. Guidi, and S. M. Bennington, Not. Neutroni Luce Sincrotrone **14**, 22 (2009).
[56] D. Inosov, Y. Onykiienko, and H. Walker, 1810530, STFC ISIS Facility, doi:10.5286/ISIS.E.90575806 (2018).
[57] J. Sichelschmidt *et al.* (unpublished).
[58] A. Abragam and B. Bleaney, *Electron Paramagnetic Resonance of Transition Ions*, Vol. 1 (Clarendon, Oxford, UK, 1970).
[59] S. Lausberg, A. Hannaske, A. Steppke, L. Steinke, T. Gruner, L. Pedrero, C. Krellner, C. Klingner, M. Brando, C. Geibel, and F. Steglich, Phys. Rev. Lett. **110**, 256402 (2013).
[60] S. Yamashita, Y. Nakazawa, M. Oguni, Y. Oshima, H. Nojiri, Y. Shimizu, K. Miyagawa, and K. Kanoda, Nat. Phys. **4**, 459 (2008).
[61] Y.-D. Li, Y. Shen, Y. Li, J. Zhao, and G. Chen, Phys. Rev. B **97**, 125105 (2018).
[62] X. Zhang, F. Mahmood, M. Daum, Z. Dun, J. A. M. Paddison, N. J. Laurita, T. Hong, H. Zhou, N. P. Armitage, and M. Mourigal, Phys. Rev. X **8**, 031001 (2018).
[63] W. Liu, Z. Zhang, J. Ji, Y. Liu, J. Li, X. Wang, H. Lei, G. Chen, and Q. Zhang, Chin. Phys. Lett. **35**, 117501 (2018).